CrystEngComm

Accepted Manuscript

ROYAL SOCIETY OF CHEMISTRY

www.rsc.org/crystengcomm

CrystEngComm RSCPublishing

ARTICLE

Ab initio modeling of single wall nanotubes folded from α- and γ-V_2O_5 monolayers: structural, electronic and vibrational properties

Cite this: DOI: 10.1039/x0xx00000x

V.V. Porsev,[a] A. V. Bandura[a] and R. A. Evarestov[a]

Received ooth January 2015,
Accepted ooth January 2015

DOI: 10.1039/x0xx00000x

www.rsc.org/

We have performed first-principles calculations of the atomic and electronic structure of single wall nanotubes (NTs) of the two possible chirality types rolled up from monolayers of α- and γ-V_2O_5 phases. We have used a hybrid exchange–correlation PBE0 functional within the density functional theory and a basis set of localized atomic orbitals. A dispersion correction has been taken into account. All the lattice parameters and the atomic positions have been totally optimized. The strain energies calculated for nanotubes folded from layers of both phases along the [100] direction are close to zero. This reflects the unique flexibility of the layers for folding in the [100] direction. The electronic structure of both phase nanotubes appeared to be similar to that of the parent layer. It was found that for both considered phases the nanotubes of the same chirality are energetically equivalent but the shape of γ-NTs is closer to cylindrical form than that of α-NTs. Young's moduli calculated for (6,0) α- and γ-NTs were found to be 172 GPa and 148 GPa, respectively. Phonon mode frequencies of (6,0) α- and γ-NTs have been calculated and compared with those of α- and γ-V_2O_5 free layers.

1. Introduction

Vanadium(V) oxide is an important crystalline compound which is employed as a catalyst in many industrial areas.[1] The numerous nanostructures of vanadia such as nanotubes or nanoscrolls,[2] nanorods,[3] fullerene analogues,[4] or more exotic nanourchins[5] and various nanorings[6] have been synthesized. These nanostructures are the subject of intensive experimental investigations due to perspective future applications. Nanotubes of V_2O_5 exhibit the various structures. One of the forms of nanotubes and nanoscrolls (VO_x) is composed of the mixed-valence vanadate anions (V_7O_{16}) and the protonated organic amines as a template.[7] Another two types of synthesized NTs are the following: nanotube array which consists from amorphous V_2O_5;[8,9] nanocables composed of carbon nanotubes (CNT) covered by ultrathin V_2O_5 shell being perspective materials for supercapacitors.[10,11] A monolayer-thick V_2O_5 shell can be grown at CNT from molten V_2O_5 using surface-tension effect.[12]

While the properties of the bulk V_2O_5 phases and their free layers are well studied theoretically (see Refs. 13–15 and references therein), only few simulations[16–18] are performed on α-V_2O_5 based nanotubes. Electronic properties of single wall nanotubes[16] and nanoscrolls[17] rolled up from α-V_2O_5 were calculated by semiempirical extended Hückel theory. The main result obtained in these calculations – the decreasing of the band gap to zero with decreasing of the diameter of nanotube or nanoscroll. The geometry optimization of nanotubes is not performed in Refs. 16,17. However the optimized atomic structure and nanotube properties can considerably differ from the initial one derived from the bulk structure of α-V_2O_5. The nanotube structure optimization was made by Zhu at al.[18] to investigate CO oxidation on α-V_2O_5 nanotubes. It was demonstrated the importance of the vanadia layer curvature.

In our recent publication[19] we have performed first-principles calculations of the optimized atomic structure, electronic properties and stability of two (α and γ) bulk V_2O_5 phases and their free layers within the same computational approach. The orthorhombic α-V_2O_5 (*Pmmn*) is the most stable phase of vanadia.[20] The orthorhombic γ-V_2O_5 (*Pnma*) is metastable phase which can be prepared by deintercalation of lithium from γ-LiV_2O_5.[21] Although the formation energy of the bulk γ-V_2O_5 is 11 kJ/mol higher than that of the bulk α-V_2O_5, the formation energies of monolayers of α- and γ-V_2O_5 are very close, and both these layers potentially can be easily rolled up due to their flexibility.[19] The close values of monolayer formation energies of both phases result in existence of γ-V_2O_5 at nanoscale level. The formation of γ-V_2O_5 nanorods was experimentally observed.[22,23] Authors of Ref. 5 assign some vibrations in the vanadia nanotubes to the vibrations of bulk γ-V_2O_5.

In the present paper we consider for the first time the structural, electronic and vibrational properties of the fully optimized single wall nanotubes of different chirality types rolled up from monolayers of both the α- and γ-V_2O_5 phases. The latter was never considered before.

The structure of this paper is as follows. Section 2 describes theoretical backgrounds of nanotube folding and computational details of our calculations. Section 3 reports the results obtained for structural, electronic and vibrational properties of nanotubes folded from α- and γ-V_2O_5 phases. Finally, we summarize with conclusions in Section 4.

2. Theoretical backgrounds and computational details

The nanotube symmetry and structure can be described using layer folding which means the construction of the cylindrical surfaces of nanotubes by rolling up the two-periodic (2D) crystalline layers.

Let **a** and **b** be the primitive translation vectors of the 2D lattice of the layer and γ the angle between them. To specify the symmetry of nanotubes as monoperiodic (1D) systems, it is necessary to define a finite 1D translation vector $\mathbf{L} = l_1\mathbf{a} + l_2\mathbf{b}$ along the nanotube axis and a chiral vector $\mathbf{R} = n_1\mathbf{a} + n_2\mathbf{b}$ (l_1, l_2, n_1, and n_2 are integers). The nanotube of the chirality (n_1, n_2) is obtained by folding the layer in a way that the chiral vector **R** becomes the circumference of the nanotube. To provide translational periodicity these two vectors must be mutually orthogonal, (**R**·**L**) = 0. Orthogonality condition can be written in the following form:

$$\frac{l_1}{l_2} = -\frac{n_2 b^2 + n_1 ab\cos(\gamma)}{n_1 a^2 + n_2 ab\cos(\gamma)}. \quad (1)$$

The (001) layers of α- and γ-V_2O_5 (hereinafter α-layer and γ-layer) possess a primitive rectangular lattice with $a \neq b$, γ = 90° for which the orthogonality condition turns to

$$\frac{l_1}{l_2} = -\frac{n_2 b^2}{n_1 a^2}, \quad (2)$$

with only two possible solutions $n_1 \neq 0$, $n_2 = 0$, and $n_1 = 0$, $n_2 \neq 0$. So, the chirality types which are compatible with the 1D periodicity are only the (n_1, 0) and (0, n_2) (see Fig. 1).[24]

It should be noted that authors of some papers[16–18] erroneously transferred the symmetry classification of carbon nanotubes folded from the graphene hexagonal lattice to those folded from the rectangular one. For example, the rectangular (n_1, 0) chiralities of V_2O_5 NTs were incorrectly designated as the hexagonal-derived armchair (n, n) chiralities, and the rectangular (0, n_2) chiralities were designated as the hexagonal-derived zigzag (n, 0) chiralities.

In the present calculations, we have used the hybrid density functional theory – Hartree-Fock (DFT-HF) method with the PBE0 exchange-correlation functional.[25,26] Apart from a band gap, other properties under consideration are well predictable by hybrid functionals. We have performed all computations using a basis set of Gaussian atomic orbitals implemented in the CRYSTAL09 computer code.[27,28] For O and V atoms we used a full electron consistent portable basis set of the triple-zeta valence with the polarization quality, pob-TZVP.[29] A feature of this basis set is portability between various solid state systems. To take into account the dispersion interactions (important for the layered structures description), we have applied the empirical Grimme correction[30] DFT-D implemented in CRYSTAL09. The scaling factor s_6 corresponded to the calculation of Grimme correction using PBE0 is set to 0.5 according to Ref. 31, whereas the steepness d and cutoff radius R_{cut} for direct lattice summation are equal to 20 and 25.0 Å, respectively.

Unfortunately, the DFT-D correction adds more empiricism to DFT. We cannot estimate an exact contribution of dispersion interactions into the energy to verify the correctness of DFT-D approach. Due to this fact, here we present the data of both DFT and DFT-D versions of the calculations.

A high tolerance of 10^{-9} was used in the direct lattice summations for the overlap threshold in one-electron integrals, for the overlap and the penetration threshold in Coulomb integrals and for overlap threshold in exchange integrals. For the truncation of lattice exchange series, two different pseudo-overlap thresholds were used (10^{-10} and 10^{-18}) according to different roles of two summations in the self-consistent stage.[27] Kohn–Sham equations were solved iteratively to self-consistency within 3×10^{-7} and 3×10^{-8} eV for nanotubes and bulk phases respectively. The Monkhorst–Pack scheme[32] with 12 and 4 **k**-point mesh was applied in Brillouin zone (BZ) sampling in calculations of nanotubes with (n_1, 0) and (0, n_2) chirality types, respectively. To obtain ground state properties the lattice parameters and fractional positions of atoms were fully optimized. Relaxations were achieved with the convergence criterion for the forces on atoms set to 0.015 eV·Å^{-1} and 0.005 eV·Å^{-1} for nanotubes and bulk phases, respectively.

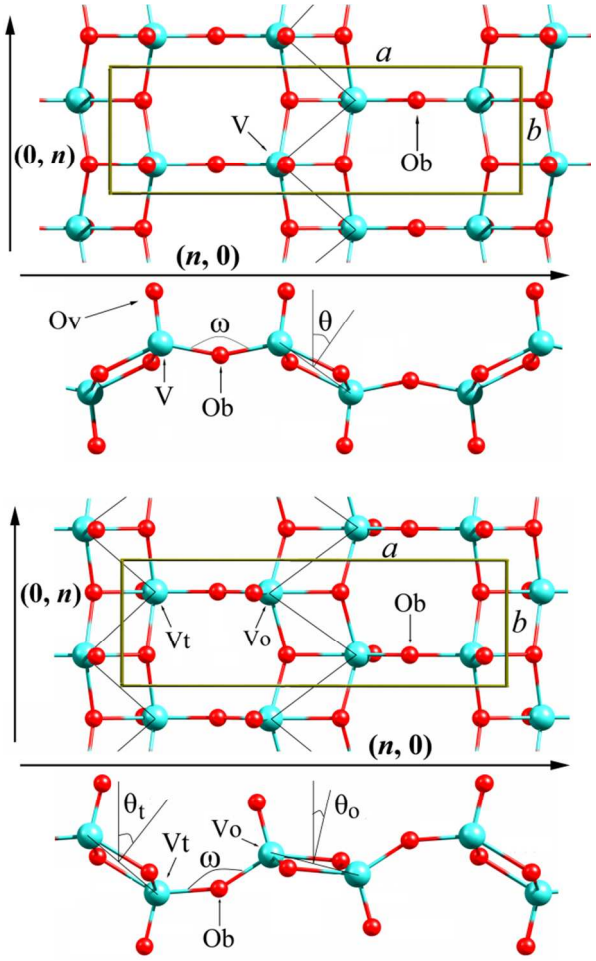

Figure 1. The [001] and [010] views of α-V_2O_5 (top) and γ-V_2O_5 (bottom) free (001) layers optimized by PBE0. Possible ways of layer folding are denoted by arrows. The black line connects vanadium atoms of zigzag chains. Legend: V, large balls; O, small balls.

The zone-center phonon frequencies are determined from the numerical second order derivatives of the ground state energy using the analytical first derivatives and the finite displacement method adopted for the harmonic frequency calculation in CRYSTAL09 code.[33]

3. Results and discussion

The comparison of our results of previous[19] PBE0 and present PBE0-D calculations of bulk phases and free layers with experimental data is presented in Table 1 for α- and γ-V_2O_5. It can be seen that an account of dispersion forces results in some decrease of lattice parameters. It should be noted that the optimized structures of both considered phases demonstrate a

good agreement with the experimental observations for both DFT and DFT-D computational schemes. Computed enthalpy of atomization of α-V_2O_5 is very close to experimental value as well. Formation energies of bulk γ-V_2O_5 are close to each other in DFT and DFT-D. However, accounting of dispersion forces adds about 20 kJ/mol to layer formation energies, thus putting them into the theoretical range estimated in ref. 34. Nevertheless, α- and γ-layers are remaining to be energetically equivalent using both calculation schemes and this is the reason to consider nanotubes obtained with folding the layers of both phases.

A layer group number of the α-layer is 46 (*Pmmn*).[35] The primitive 2D unit cell of the α-layer contains two formula units and four types of nonequivalent atoms: one vanadium atom and three different types of oxygen atoms. The atomic structure of the α-layer consists of edge-shared distorted square pyramids of VO_5, forming zigzag chains in the [010] direction. Each chain can be characterized by the angle θ between the normal to the (001) plane and the normal to a plane formed by three vanadium atoms interconnected within the chain. Chains are connected by the bridging oxygen atoms Ob in the [100] direction with the bond angle ω (see Fig. 1).

The layer group number of the γ-layer is 15 ($P2_1/m11$),[35] it contains two formula units in the primitive cell and seven types of nonequivalent atoms (five oxygen and two vanadium atom types). Two nonequivalent zigzag chains are extended in [010] direction and characterized by the two angles θ_o and θ_t. These chains are connected by bridging oxygen atoms Ob in the [100] direction with the bond angle ω (see Fig. 1). Atomic structure of γ-layer is different using PBE0 and PBE0-D calculations. Optimization with PBE0 gives flattening of γ-layer, while accounting of dispersion forces leads to twisted layers as in bulk γ-V_2O_5.

Fully optimized structures of α- and γ-layers have been used for NTs folding with chiralities (n_1, 0) and (0, n_2). The choice of n_1 in the interval from 2 to 16 provides NT average diameters from 10 to 56 Å (see Tables 2 and 3 for details). The average diameters of considered (0, n_2) NTs change from 10.5 Å to 28 Å.

The folding procedure results in splitting of the layer atom types, bond distances, and angles into inward (in) and outward (out) types. Four atom types within the α-layer and seven ones within the γ-layer are converted into eight and fourteen atom types in α- and γ-NTs respectively. Examples of fully optimized structures of α- and γ-NTs are presented at Figs. 2 and 3. The α-NTs of both chirality types belong to the 11th family of line symmetry groups (*Ln/mmm* or $L\overline{2n}2m$ for even or odd *n*, respectively).[37] The γ-NTs of (n_1, 0) and (0, n_2) chirality types belong to 3rd (*Ln/m* or $L\overline{2n}$ for even or odd *n*, respectively) and 6th (*Lnmm* or *Lnm* for even or odd *n*, respectively) families of line symmetry groups, correspondingly.[37]

Table 1. Properties of V_2O_5 various phases.

	a,[a] Å	b,[a] Å	c,[a] Å	β,[a] °	ω,[b] °	θ,[b] °	E_{form}[c]	E_{gap}[d]	E_{cgap}[d]
					α-V_2O_5				
Bulk, exp.[20]	11.544	3.571	4.383	90	149.2	22.2	0	2.3[36]	–
Bulk, PBE0[19]	11.471	3.546	4.396	90	149.3	22.9	0	4.0	0.7
Bulk, PBE0-D	11.507	3.528	4.298	90	150.3	22.6	0	4.0	0.7
Layer, PBE0[19]	11.076	3.562	–	–	157.7	34.3	20	4.3	0.7
Layer, PBE0-D	11.199	3.538	–	–	151.2	30.5	42	4.4	0.7
					γ-V_2O_5				
Bulk, exp.[21]	9.946	3.585	10.042	90	124.4	7.6(o)[e], 55.7(t)[e]	–	–	–
Bulk, PBE0[19]	10.055	3.565	10.232	90	129.0	4.7(o), 55.3(t)	11	4.2	0.7
Bulk, PBE0-D	10.001	3.548	9.945	90	127.8	6.4(o), 56.3(t)	11	4.2	0.7
Layer, PBE0[19]	10.855	3.561	–	–	151.2	12.7(o), 40.2(t)	21	4.3	0.8
Layer, PBE0-D	10.245	3.542	–	–	131.2	4.2(o), 45.4(t)	41	4.3	0.7

[a] lattice parameters;
[b] see Fig. 1;
[c] formation energy, kJ/mol;
[d] E_{gap} is band gap, eV; E_{cgap} is gap in conduction band, eV;
[e] for (o) and (t) designations see Fig. 1 and ref. 19.

The optimization of the (n_1, 0) α- and γ-NTs structure leads to minor changes of bond distances (by a few thousandths of Angstrom). Changes of angles ω are more considerable. For low values of n_1 (see Tables 2 and 3) the values of ω_{out} exceed 180°. In other words, initially concave angles mute to convex angle during optimization process. The appreciable change of ω is accompanied by the change of θ. Such behavior of angles ω and θ reflects the unique flexibility of the α-layer during the rolling along the *a* direction. The bending stress in NTs is neutralized by the almost effortless changing of ω and θ angles.

Elimination of the bending tensions provides the very low strain energies E_{str} of (n_1, 0) α- and γ-NTs. Strain energy can be considered as the nanotube formation energy from the corresponding layer with the optimized structure (per formula unit):

$$E_{\mathrm{str}} = \frac{E_{\mathrm{NT}}}{n_{\mathrm{NT}}} - \frac{E_{\mathrm{slab}}}{n_{\mathrm{slab}}}, \qquad (3)$$

where E_{NT}, n_{NT} and E_{slab}, n_{slab} are the total energy and the number of formula units in the NT and layer unit cells, correspondingly. Our values of E_{str} for (n_1, 0) α-NTs are close to those calculated in ref. 18 for n_1 from 3 to 8.

Flexibility of nanolayers in the [100] direction is reflected by low strain energies of the corresponding NTs. Thus, calculated strain energy of (n_1, 0) α-NTs becomes about 1 kJ/mol or less for $n_1 \geq 9$. Flexibility of γ-layers is even greater: PBE0 calculations result in zero strain energies of (n_1, 0) γ-NTs for $n_1 > 4$. The initial "up-down-up-down" alternation of vanadyl oxygen atoms in the γ-layer provides the structure which is more appropriate for folding into NTs than the "up-up-down-down" alternation in the α-layer. Next, the two neighbor "down-down" vanadyl oxygen atoms are shifted relative each other by a half of translational period. Both circumstances lead to the decrease of the oxygen-oxygen repulsion on the internal NT surface. As a consequence, the shape of γ-NTs is closer to cylindrical form than the shape of α-NTs. A more round shape can provide a more regular distribution of strains on NT circumference. All considered factors promote the stability of (n_1, 0) γ-NTs at low n_1. Thus, we were able to optimize the

narrow (2, 0) γ-NT without any reconstruction of $(V_2O_4)_n$ zigzag chains.

Strain energies calculated by PBE0 and PBE0-D computational schemes are close (Tables 2 and 3). Contribution of the dispersion forces is essential only for small n_1. The dispersion interactions decrease the strain energies of nanotubes with small diameters presumably because of relative proximity of their opposite sides.

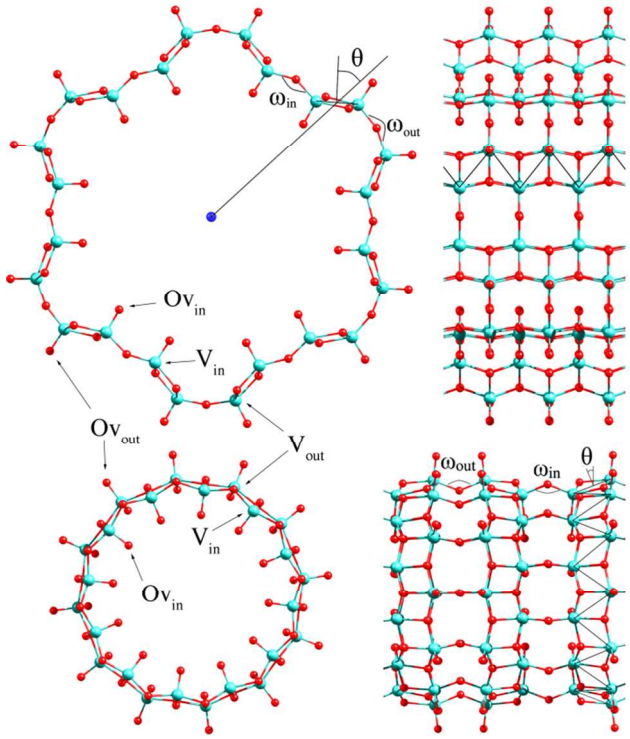

Figure 2. PBE0 optimized structure of nanotubes generated from α-V_2O_5 with (n_1, 0) (top) and (0, n_2) (bottom) chiralities, n_1 = 6, n_2 = 12. The black line connects vanadium atoms of zigzag chains. See Fig. 1 for legend.

The strain energies of (0, n_2) NTs are considerably higher than those of (n_1, 0) NTs for both the considered phases. Folding of α- and γ-layers to the (0, n_2) NTs requires bending of the $(V_2O_4)_n$ zigzag chains. These parallel chains with the $(V_2O_2)_n$ covalently bonded skeleton are noticeably more rigid than V–O_b–V bridging groups between them. Hence, it is impossible to reduce the bending stress in (0, n_2) NTs by appropriate tuning of angles θ or ω as it occurs in (n_1, 0) NTs. As a result, the bond distances in (0, n_2) NTs are altered in more extent than in (n_1, 0) NTs, although their deviations from the layer values do not exceed a few hundredths of Angstrom. Differences in strain energies of (0, n_2) NTs calculated by both computational schemes are small. Diameters of all considered (0, n_2) NTs are sufficiently large and dispersion interaction between opposite sides of wall is negligible.

Let us consider the rolling-up process and the subsequent relaxation of the γ-NT in detail. Just after rolling, all the atoms of the layer are distributed between two groups: inward and outward atoms, so the seven types of atoms in γ-layer turn into the fourteen atom types in γ-NT (due to disappearance of the inversion operation). However, during the structure optimization the number of nonequivalent atoms reduces again to seven because of appearance of the new symmetry element, namely a screw axis. The new screw rotation axis of order $2n_1$ interchanges the position of atoms of (o) and (t) types (see Figs. 1 and 3) and provides the change of the line group family from 3th to 4th.[37]

The enhancement of the symmetry can be traced by the difference between the angles θ_o and θ_t which decreases from 27.5° in the γ-layer to practically zero in the optimized γ-NT structure (see Table 3). The difference between the angle ω_{in} and the angle complementary to ω_{out} (i.e. 360°– ω_{out}) reveals the similar behavior. Simultaneously, the optimization of (0, n_2) γ-NTs results in transformation of their symmetry from the 6th to the 8th family of line groups.[37]

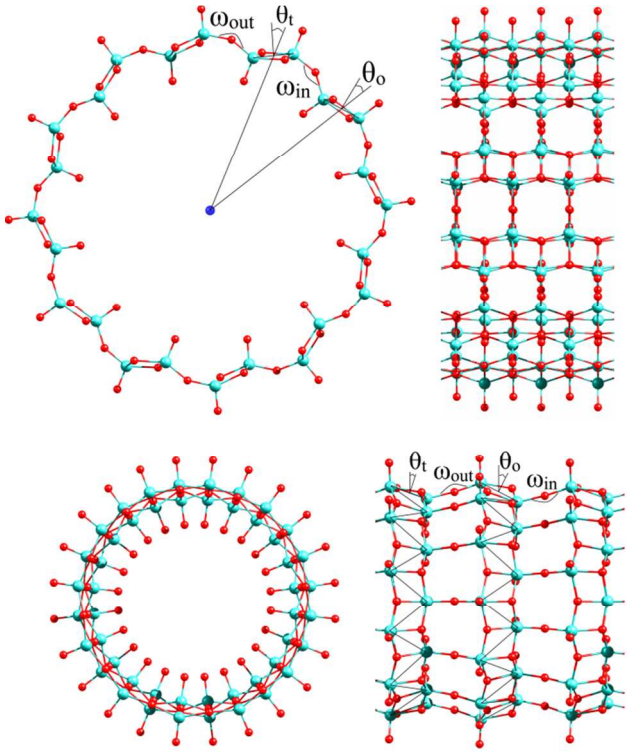

Figure 3. PBE0 optimized structure of nanotubes generated from γ-V_2O_5 with (n_1, 0) (top) and (0, n_2) (bottom) chiralities, n_1 = 6, n_2 = 12. The black line connects vanadium atoms of zigzag chains. See Fig. 1 for legend.

As mentioned above, the strain energy of nanotubes is calculated relative to a parent layer. To compare the energetic stability of nanotubes folded from various layers, it is necessary to compare the formation energy of nanotubes:

$$E_{\text{form}} = \frac{E_{\text{NT}}}{n_{\text{NT}}} - \frac{E(\alpha\text{-}V_2O_5)_{\text{bulk}}}{n(\alpha\text{-}V_2O_5)_{\text{bulk}}}. \quad (4)$$

Inclusion of dispersion forces does not change the relative energetic stability of nanotubes. It only shifts the formation energy to higher values (by about 20 kJ/mol). Due to this reason in Fig. 4 we present the formation energy dependence obtained by PBE0-D calculation only.

Figure 4 shows that the formation energy difference between α- and γ-NTs is negligible at large chirality indices for both chirality types. So, in this case the nanotubes obtained from both phases are energetically equivalent. In the case of (n_1, 0) chirality type with small indices n_1 the γ-NTs are more stable than the α-NTs, while opposite is true for (0, n_2) chirality type with small indices n_2.

CrystEngComm RSCPublishing

ARTICLE

Table 2. Properties of selected α-V_2O_5 nanotubes.

chirality	D,[a] Å	t,[a] Å	E_{form}[b]	E_{str}[b]	E_{gap}[c]	E_{cgap}[c]	θ,[d] °	ω_{in},[d] °	ω_{out},[d] °
				NT (n_1, 0)					
(3, 0)	10.3 (10.3)	3.55 (3.52)	34 (52)	14 (10)	4.3 (4.3)	0.6 (0.6)	44.2 (44.7)	135.1 (134.8)	210.3 (215.3)
(4, 0)	13.3 (13.2)	3.56 (3.53)	25 (44)	5 (3)	4.3 (4.3)	0.7 (0.7)	47.2 (48.4)	143.6 (143.5)	213.1 (218.1)
(6, 0)	20.3 (19.8)	3.56 (3.54)	22 (43)	3 (1)	4.3 (4.3)	0.7 (0.7)	43.3 (47.0)	149.2 (152.6)	200.0 (210.0)
(10, 0)	34.9 (35.0)	3.56 (3.54)	21 (43)	1 (1)	4.3 (4.3)	0.7 (0.7)	37.5 (36.4)	150.3 (147.8)	177.8 (177.4)
(16, 0)	56.2 (56.7)	3.56 (3.54)	21 (43)	1 (1)	4.3 (4.3)	0.7 (0.7)	35.6 (33.0)	152.0 (147.7)	168.3 (163.6)
				NT (0, n_2)					
(0, 9)	10.4 (10.4)	11.31 (11.32)	72 (91)	51.7 (49)	4.4 (4.5)	0.3 (0.3)	12.4 (12.4)	131.5 (130.7)	134.7 (133.9)
(0, 10)	11.5 (11.4)	11.33 (11.34)	60 (79)	40.3 (37)	4.4 (4.4)	0.3 (0.3)	14.1 (13.6)	133.1 (132.4)	135.3 (134.6)
(0, 16)	18.1 (18.0)	11.34 (11.37)	35 (55)	14.9 (13)	4.3 (4.4)	0.5 (0.5)	20.8 (19.8)	141.6 (139.9)	139.3 (138.0)
(0, 25)	28.2 (28.1)	11.28 (11.32)	26 (47)	6.2 (5)	4.3 (4.3)	0.6 (0.6)	25.8 (24.3)	149.0 (145.9)	143.4 (141.3)

Numbers in parentheses are results of PBE-D calculations;
[a] D is average diameter estimated as sum of radial distances to outmost and innermost oxygen atoms, t is translational period;
[b] E_{form} is formation energy, kJ/mol; E_{str} is strain energy, kJ/mol;
[c] E_{gap} is band gap, eV; E_{cgap} is gap in conduction band, eV;
[d] see Figs. 1 and 2.

Table 3. Properties of selected γ-V_2O_5 nanotubes.

chirality	D,[a] Å	t,[a] Å	E_{form}[b]	E_{str}[b]	E_{gap}[c]	E_{cgap}[c]	θ_o; θ_t,[d] °	ω_{in},[d] °	ω_{out},[d] °
				NT(n_1, 0)					
(2, 0)	7.0 (7.0)	3.54 (3.52)	45 (59)	25 (18)	4.5 (4.5)	0.8 (0.7)	24.1 (24.4); 24.0 (24.3)	114.5 (114.5)	245.5 (245.4)
(3, 0)	10.3 (10.2)	3.56 (3.54)	25 (42)	4 (1)	4.4 (4.4)	0.7 (0.7)	26.6 (26.6); 26.6 (26.5)	127.3 (124.7)	232.6 (235.4)
(4, 0)	13.8 (13.8)	3.56 (3.54)	22 (41)	1 (0)	4.3 (4.3)	0.7 (0.7)	26.5 (26.3); 26.7 (26.3)	137.2 (133.7)	222.6 (226.3)
(6, 0)	21.0 (20.9)	3.56 (3.54)	21 (42)	0 (1)	4.3 (4.3)	0.8 (0.7)	24.9 (25.2); 27.9 (27.2)	146.2 (143.1)	208.4 (213.2)
(10, 0)	35.2 (33.5)	3.56 (3.54)	21 (42)	0 (1)	4.3 (4.3)	0.8 (0.7)	22.5 (5.9); 30.4 (46.9)	152.0 (126.2)	192.2 (153.3)
(16, 0)	55.9 (53.4)	3.56 (3.54)	21 (42)	0 (1)	4.3 (4.3)	0.8 (0.7)	16.0 (5.1); 36.9 (47.6)	147.2 (129.9)	169.5 (145.0)
				NT(0, n_2)					
(0, 9)	10.6 (10.5)	11.30 (11.31)	91 (113)	70 (72)	4.3 (4.3)	0.7 (0.7)	21.5 (21.2); 21.4 (21.3)	181.9 (183.1)	178.2 (176.7)
(0, 10)	11.6 (11.5)	11.29 (11.30)	72 (95)	52 (54)	4.4 (4.3)	0.7 (0.7)	22.2 (22.0); 22.3 (22.1)	183.7 (185.5)	176.0 (174.4)
(0, 16)	18.1 (18.0)	11.23 (11.24)	35 (57)	14 (16)	4.3 (4.4)	0.8 (0.8)	24.0 (24.9); 25.5 (24.3)	185.5 (188.7)	171.0 (169.5)
(0, 25)	28.3 (28.1)	11.21 (11.21)	25 (47)	5 (6)	4.3 (4.3)	0.8 (0.8)	25.0 (26.2); 26.3 (25.0)	185.0 (187.4)	171.9 (169.7)

Numbers in parentheses are results of PBE-D calculations;
[a] D is average diameter estimated as sum of radial distances to outmost and innermost oxygen atoms, t is translational period;
[b] E_{form} is formation energy, kJ/mol; E_{str} is strain energy, kJ/mol;
[c] E_{gap} is band gap, eV; E_{cgap} is gap in conduction band, eV;
[d] see Figs. 1 and 3.

CrystEngComm RSCPublishing

ARTICLE

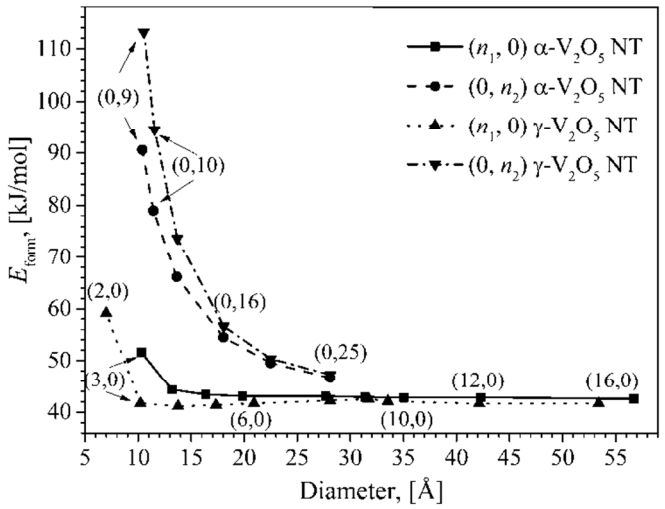

Figure 4. Formation energies of α- and γ-V_2O_5 nanotubes with (n_1, 0) and (0, n_2) chiralities calculated with PBE0-D.

Next, we have estimated the Young's moduli Y of (n_1, 0) α- and γ-NTs at n_1 = 6 using PBE0 functional. The Young's moduli have been calculated using the second derivative of the energy E with respect to the strain $\varepsilon_{||}$ at the equilibrium volume V_0:[38]

$$Y = \frac{1}{V_0} \times \frac{\partial^2 E}{\partial \varepsilon_{||}^2}, \quad V_0 = \pi D_0 t_0 h, \quad \varepsilon_{||} = \frac{t}{t_0} - 1, \qquad (5)$$

where D_0 is an average diameter, h is the thickness of the layer, t_0 and t are periods of unstrained and strained nanotube, accordingly. The thickness h is assumed to be equal to the optimized lattice parameter c of bulk α-V_2O_5 and c/2 of bulk γ-V_2O_5. The obtained values of Y are equal to 172 and 148 GPa for (6, 0) α- and γ-NT, respectively. So, we can see that the stiffness of α-NT is higher than that of γ-NT. The measured values of Young's modulus of VO_x nanotubes[39] span the 20–80 GPa range but the higher values may be more intrinsic to the VO_x layers. Thus, Fateh et al.[40] reported that with the increase in the crystallinity of the thin films of V_2O_5, Young's modulus can increase from 80 to 130 GPa. Our values are comparable with upper bound of this interval.

Let us consider the electronic density of states (DOS) of V_2O_5. Conduction zone of bulk α- и γ-V_2O_5 mainly consists of 3*d* states of vanadium with noticeable contribution of 2*p* orbitals of oxygen.[41,15] The DOS of α- и γ-layer is very similar to the bulk DOS due to weak interactions between layers in the bulk.[13,15,19] One of the features of bulk and monolayer V_2O_5 DOS is the existence of the narrow split-off conduction band which is separated from another conduction bands by a certain gap (E_{cgap}). Such split-off conduction bands exist in only a few materials. Solar cells constructed from such materials could exceed efficiency of the single gap solar cell.[42] It is worth noting that both α- and γ-V_2O_5 phases have these split-off conduction bands[41,15,19] with no doping required.

Detailed theoretical treatment of the electronic structure of α-V_2O_5[41] clearly demonstrated that peculiarities of the band structure were determined by crystal field splitting of 3*d* electronic states of vanadium due to local distorted square pyramid of oxygen atoms surrounding the vanadium atom.

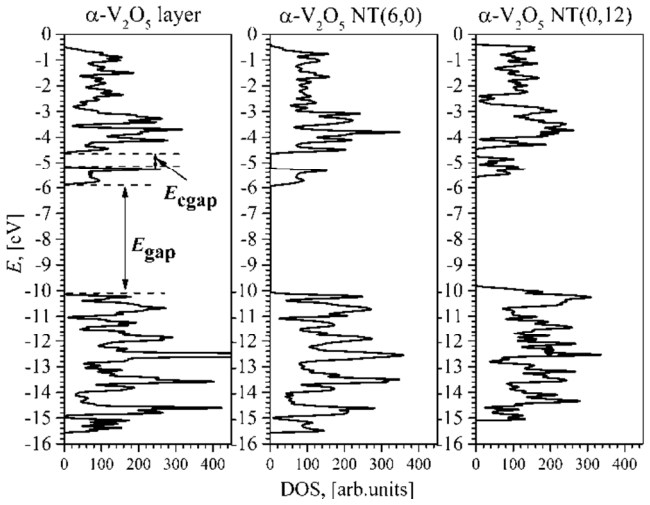

Figure 5. Total electronic DOS of free layer and nanotubes of α-V_2O_5 obtained with PBE0.

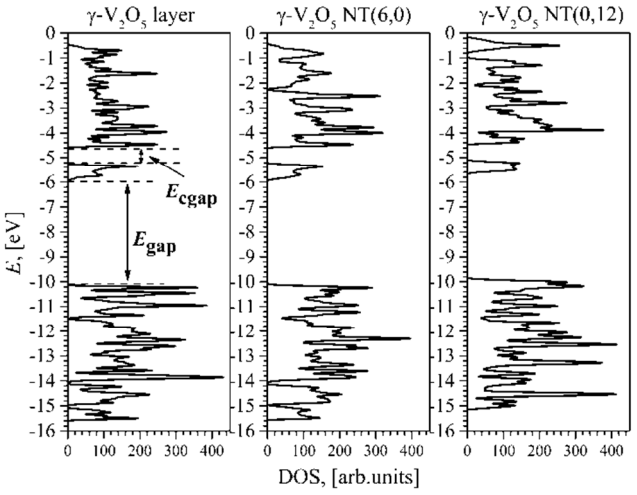

Figure 6. Total electronic DOS of free layer and nanotubes of γ-V_2O_5 obtained with PBE0.

The total DOS of α- and γ-layer and of selected α- and γ-NTs are presented in Figs. 5 and 6. The calculated DOS of optimized NTs are nearly the same as the bulk and layer DOS. This contradicts with the results of calculations[16,17] of α-V_2O_5 NTs in which the structure optimization was not made.

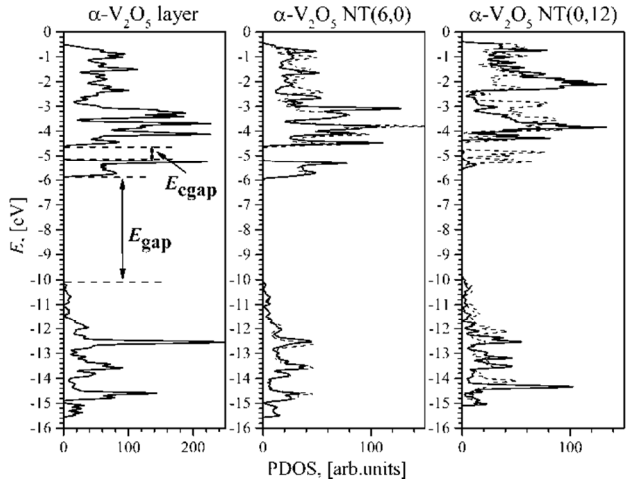

Figure 7. Vanadium 3*d* partial DOS of free layer and nanotubes of α-V_2O_5 obtained with PBE0. PDOS of outward and inward vanadium atoms are represented by solid and dashed lines, respectively.

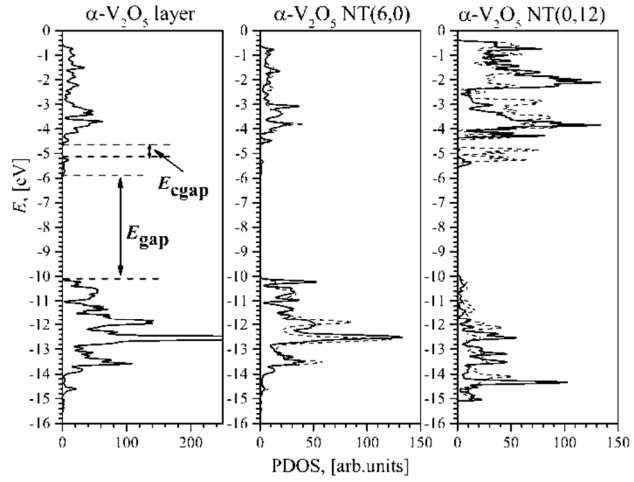

Figure 8. Vanadyl oxygen 2*p* partial DOS of free layer and nanotubes of α-V_2O_5 obtained with PBE0. PDOS of outward and inward vanadyl oxygen atoms are represented by solid and dashed lines, respectively.

Compared with the layer results the changes of E_{gap} in (n_1, 0) NTs are minor (see Tables 2, 3) except the (2, 0) γ-NT with a very small diameter where it increases by a value of 0.2 eV relative to the band gap for γ-layer.

The DOS of NTs retain the split-off conduction band. Although the band gap E_{gap} is overestimated by PBE0 hybrid exchange-correlation DFT method and underestimated by the pure DFT approach, the hybrid and pure DFT approaches give the close values of intermediate gap E_{cgap} for the bulk V_2O_5.

For the different nanotubes the values of E_{cgap} are generally similar except the case of (0, n_2) α-NTs for which E_{cgap} decreases from 0.7 eV to 0.3 eV. In Figs. 7 and 8 we show the partial density of states (PDOS) projected to vanadium 3*d* and oxygen 3*p* orbitals. According to Figs. 7 and 8, the decrease of intermediate gap in (0, n_2) α-NTs is due to broadening of PDOS of 3*d* and 3*p* states of inward type vanadium and vanadyl oxygen atoms, respectively.

The difference between PDOS of inward and outward types is negligible for other atom types in (0, n_2) α-NTs. In (n_1, 0) NTs of both phases and in (0, n_2) γ-NTs this difference is also insignificant. Nevertheless, although the more rigid (0, n_2) NTs demonstrate the more distinct variation of band gaps and PDOS, the qualitative features of the total DOS remain the same as in the free unfolded layers.

The peculiarities of the electronic structure of NTs can easily be understood by taking into account the mentioned flexibility of layers. Local square pyramid surrounding of vanadium atoms is preserved by stress-free adjusting of ω and θ angles. Only for (0, n_2) α-NTs the intermediate conduction band is broadening due to some shift of inward type vanadium atom towards the base of square pyramid (see Fig. 2). This broadening of conduction bands resembles the changes of DOS found[41] in the computationally modeled artificial V_2O_5 phase with vanadium atoms located at the base of square pyramid.

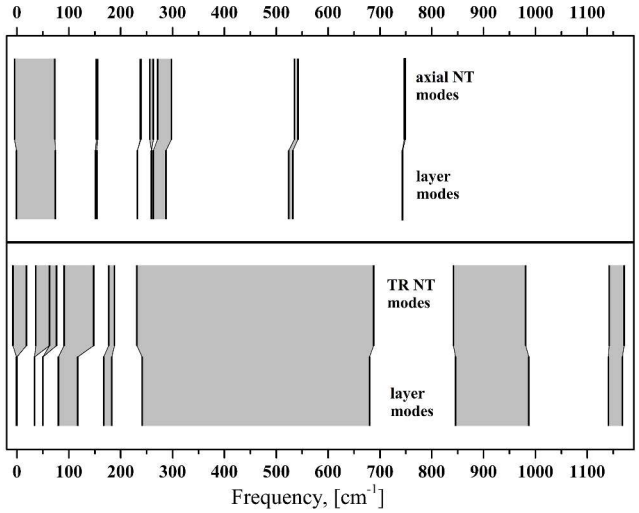

Figure 9. Mapping between groups of phonon frequencies of α-layer and (6, 0) α-NT. Upper part: axial type NT phonons; bottom part: TR (twisting-radial) type NT phonons.

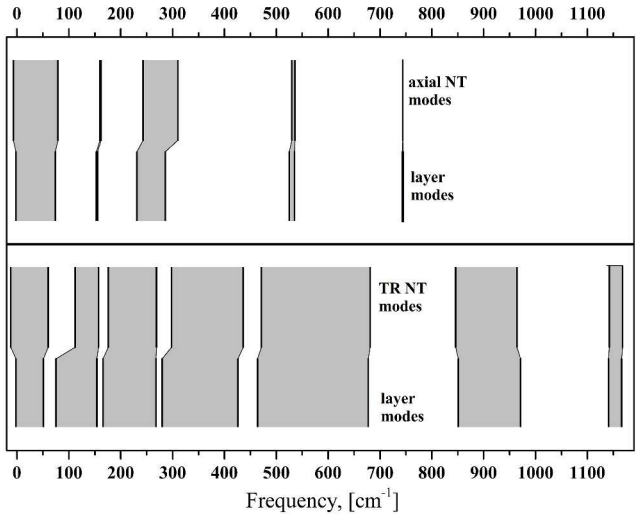

Figure 10. Mapping between groups of phonon frequencies of γ-layer and (6, 0) γ-NT. Upper part: axial type NT phonons; bottom part: TR (twisting-radial) type NT phonons.

In order to investigate the structural stability and phonon properties of the considered nanotubes we have calculated the phonon frequencies of selected NTs at Γ-point of BZ. These calculations have been made using PBE0 functional only. For this purpose we have considered the (6, 0) α- and γ-NT which belong to the line symmetry groups *L6*/*mmm* and *L6*/*m*, respectively. All calculated frequencies are positive for both nanotubes considered. This fact confirms the vibrational stability of V_2O_5 nanotubes.

The full list of phonon modes of the α- and γ-layer can be found in Ref. 19. The phonon modes of the layers (both in-plane and out of plane) at Γ-point of BZ are modified upon the folding to (6, 0) NT. The number of vibrational frequencies in (6, 0) NT are six times larger than that in the layer. The in-plane modes along the *b* direction transform to nanotube phonon modes corresponding to the vibrational motions along the nanotube axis.

The other phonon modes give rise to the twisting modes (the vibrational motion in the circumferential direction of the nanotube) and to the radial breathing modes (the vibrational motion in the radial direction of the nanotube).[43] In most cases it is difficult to assign both modes to a distinct type. Due to this fact we designate the twisting and radial breathing modes as TR (twisting-radial) modes and separate them from the axial modes.

Symmetry of (6, 0) α-NT phonon modes:
$\Gamma_{axial} = 6A_{1u} + 8A_{2u} + 7B_{1g} + 7B_{2g} + 14E_{1g} + 14E_{2u}$;
$\Gamma_{TR} = 14A_{1g} + 14A_{2g} + 14B_{1u} + 14B_{2u} + 28E_{1u} + 28E_{2g}$.

Symmetry of (6, 0) γ-NT phonon modes:
$\Gamma_{axial} = 14A_{u} + 14B_{g} + 14E_{1g} + 14E_{2u}$;
$\Gamma_{TR} = 28A_{g} + 28B_{u} + 28E_{1u} + 28E_{2g}$.

Such classification allows us to compare the layer and NT phonon modes. The analysis of normal modes with MOLDRAW graphic software[44] allows us to group similar types of frequencies of the layer and the NT. Figs. 9, 10 show correspondence obtained between these groups. It can be seen that frequency shifts caused by the layer folding are minor. This can be explained by mentioned easiness of (n_1, 0) NTs formation with preserving the local structure of the layer zig-zag chains in NTs.

4. Conclusions

Layers of α- and γ-V_2O_5 phases can be easily folded into nanotubes of the (n_1, 0) chirality with the close to zero strain energy. At large diameters the nanotubes of (n_1, 0) chirality generated from α- and γ-V_2O_5 layers are energetically equivalent. The shape of γ-NTs is closer to cylindrical form than that of α-NTs.

Nanotubes of the second possible chirality (0, n_2) are more strained due to the bending stress of the more rigid $(V_2O_4)_n$ zigzag chains. The differences between the formation energies of (0, n_2) nanotubes are negligible at large NT diameters.

The contribution of dispersion interaction is shown to be essential only for nanotubes with small diameters.

The electronic structure of V_2O_5 nanotubes reveals only small changes compared with the parent layer electronic structure due to possibility of conservation of local surrounding of vanadium atom during the geometry optimization. Some broadening of the conduction band is observed only for the most strained (0, n_2) α-V_2O_5 nanotubes.

The Young's moduli calculated for (6, 0) α- and γ-NTs are comparable with the experimental values[40] for V_2O_5 crystalline layers.

Positive values of calculated phonon frequencies confirm the vibrational stability of V_2O_5 nanotubes. The analysis of phonon modes of selected NTs shows that frequency shifts caused by the layer folding are minor.

Acknowledgements

The authors thank the Saint-Petersburg State University for a research grant 12.50.1566.2013 and highly appreciate the assistance from the Saint Petersburg State University Computer Center to make high-performance calculations.

Notes and references

[a] Department of Quantum Chemistry, St. Petersburg State University Universitetsky Prosp. 26, 198504 St. Petersburg, Petergof, Russia.

1 B.M. Weckhuysen and D.E. Keller, *Catal. Today*, 2003, **78**, 25.
2 H.-J. Muhr, F. Krumeich, U.P. Schönholzer, F. Bieri, M. Niederberger, L.J. Gauckler and R. Nesper, *Adv. Mater.,* 2000, **12**, 231.
3 B.C. Satishkumar, A. Govindaraj, M. Nath and C.N.R. Rao, *J. Mater. Chem.*, 2000, **10**, 2115.
4 R. Levi, M. Bar-Sadan, A. Albu-Yaron, R. Popovitz-Biro, L. Houben, C. Shahar, A. Enyashin, G. Seifert, Y. Prior and R. Tenne, *J. Am. Chem. Soc*., 2010, **132**, 11214.
5 C. O'Dwyer, V. Lavayen, D.A. Tanner, S.B. Newcomb, E. Benavente, G. González and C.M.S. Torres, *Adv. Funct. Mater*., 2009, **19**, 1.
6 J. Liu and D. Xue, *Nanoscale Res. Lett.*, 2010, **5**, 1619.
7 M. Wörle, F. Krumeich, F. Bieri, H.-J. Muhr and R. Nesper, *Z. Anorg. Allg. Chem.*, 2002, **628**, 2778.
8 C. Zhou, L. Mai, Y. Liu, Y. Qi, Y. Dai and W. Chen, *J. Phys. Chem. C*, 2007, **111**, 8202.
9 Y. Wang, K. Takahashi, H. Shang and G. Cao, *J. Phys. Chem. B*, 2005, **109**, 3085.
10 J.S. Bonso, A. Rahy, S.D. Perera, N. Nour, O. Seitz, Y.J. Chabal, K.J. Balkus Jr., J.P. Ferraris and D.J. Yang, *J. Power Sources*, 2012, **203**, 227.
11 I. Shakir, Z. Ali, J. Bae, J. Park and D.J. Kang, *Nanoscale*, 2014, **6**, 4125.
12 P.M. Ajayan, O. Stephan, Ph. Redlich and C. Colliex, *Nature*, 1995, **375**, 564.
13 J. Goclon, R. Grybos, M. Witko and J. Hafner, *J. Phys.:Condens. Matter*, 2009, **21**, 095008.
14 D.O. Scanlon, A. Walsh, B.J. Morgan and G.W. Watson, *J. Phys. Chem. C*, 2008, **112**, 9903.
15 M. Willinger, N. Pinna, D.S. Su and R. Schlögl, *Phys. Rev. B*, 2004, **69**, 155114.
16 V.V. Ivanovskaya, A.N. Enyashin, A.A. Sofronov, Y.N. Makurin, N.I. Medvedeva and A.L. Ivanovskii, *Solid State Commun.*, 2003, **126**, 489.
17 A.N. Enyashin, V.V. Ivanovskaya, Y.N. Makurin and A.L. Ivanovskii, *Phys. Lett. A*, 2004, **326**, 152.
18 G. Zhu, Z. Qu, G. Zhuang, Q. Xie, Q. Meng and J. Wang, *J. Phys. Chem. C*, 2011, **115**, 14806.
19 V.V. Porsev, A.V. Bandura and R.A. Evarestov, *Acta Mater.*, 2014, **75**, 246.
20 V. Shklover, T. Haibach, F. Ried, R. Nesper and P. Novák, *J. Solid State Chem.*, 1996, **123**, 317.
21 J.M. Cocciantelli, P. Gravereau, J.P. Doumerc, M. Pouchard and P. Hagenmuller, *J. Solid State Chem.*, 1991, **93**, 497.
22 N. Pinna, U. Wild, J. Urban and R. Schlögl, *Adv. Mater.*, 2003, **15**, 329.
23 N. Pinna, M. Willinger, K. Weiss, J. Urban and R. Schlögl, *Nano Lett.*, 2003, **3**, 1131.
24 R.A. Evarestov, Quantum Chemistry of Solids: LCAO Treatment of Crystals and Nanostructures, second ed. Springer Series in Solid-State Sciences 153. Berlin, Heidelberg: Springer; 2012.

25 J.P. Perdew, K. Burke and M. Ernzerhof, *J. Chem. Phys.*, 1996, **105**, 9982.
26 C. Adamo and V. Barone, *J. Chem. Phys.*, 1999, **110**, 6158.
27 R. Dovesi, V.R. Saunders, C. Roetti, R. Orlando, C.M. Zicovich-Wilson, F. Pascale, B. Civalleri, K. Doll, N.M. Harrison, I.J. Bush, P. D'Arco and M. Llunell, CRYSTAL09 User's Manual. University of Torino. Torino; 2010.
28 R. Dovesi, R. Orlando, B. Civalleri, C. Roetti, V.R. Saunders and C.M. Zicovich-Wilson, *Comput. Crystallogr.*, 2005, **220**, 571.
29 M.F. Peintinger, D.V. Oliveira and T. Bredow, *J. Comput. Chem.*, 2013, **34**, 451.
30 S. Grimme, *J. Comput. Chem.*, 2006, **27**, 1787.
31 A.V. Bandura, R.A. Evarestov and S.I. Lukyanov, *Phys. Chem. Chem. Phys.*, 2014, **16**, 14781.
32 H.J. Monkhorst and J.D. Pack, *Phys. Rev. B*, 1976, **13**, 5188.
33 F. Pascale, C.M. Zicovich-Wilson, F.L. Cejo, B. Civalleri, R. Orlando and R. Dovesi, *J. Comput. Chem.*, 2004, **25**, 888.
34 E. Londero and E. Schröder, *Phys. Rev. B*, 2010, **82**, 054116.
35 Bilbao crystallographic server: http://www.cryst.ehu.es
36 I. Loa, A. Grzechnik, U. Schwarz, K. Syassen, M. Hanfland and R.K. Kremer, *J. Alloys Compd.*, 2001, **317–318**, 103.
37 M. Damnjanović and I. Milošević, Line Groups in Physics: Theory and Applications to Nanotubes and Polymers. Lecture Notes in Physics, 801. Berlin Heidelberg: Springer Verlag; 2010.
38 T. Lorenz, D. Teich, J.-O. Joswig and G. Seifert, *J. Phys. Chem. C*, 2012, **116**, 11714.
39 B. Sipos, M. Duchamp, A. Magrez, L. Forró, N. Barišić, A. Kis, J.W. Seo, F. Bieri, F. Krumeich, R. Nesper and G. R. Patzke, *J. Appl. Phys.*, 2009, **105**, 074317.
40 N. Fateh, G. A. Fontalvo and C. Mitterer, *J. Phys. D: Appl. Phys.*, 2007, **40**, 7716.
41 V. Eyert and K.-H. Höck, *Phys. Rev. B*, 1998, **57**, 12727.
42 A. Luque, A. Marti and C. Stanley, Nat. Photonics, 2012, **6**, 146.
43 M.S. Dresselhaus and P.C. Eklund, *Adv. in Physics*, 2000, **49**, 705.
44 P. Ugliengo, D. Viterbo and G. Chiari, *Z. Crystallogr.*, 1993, **207**, 9.

Atomic, electronic and vibration properties of the single wall α- and γ-V_2O_5 nanotubes of possible chiralities have been computationally investigated.

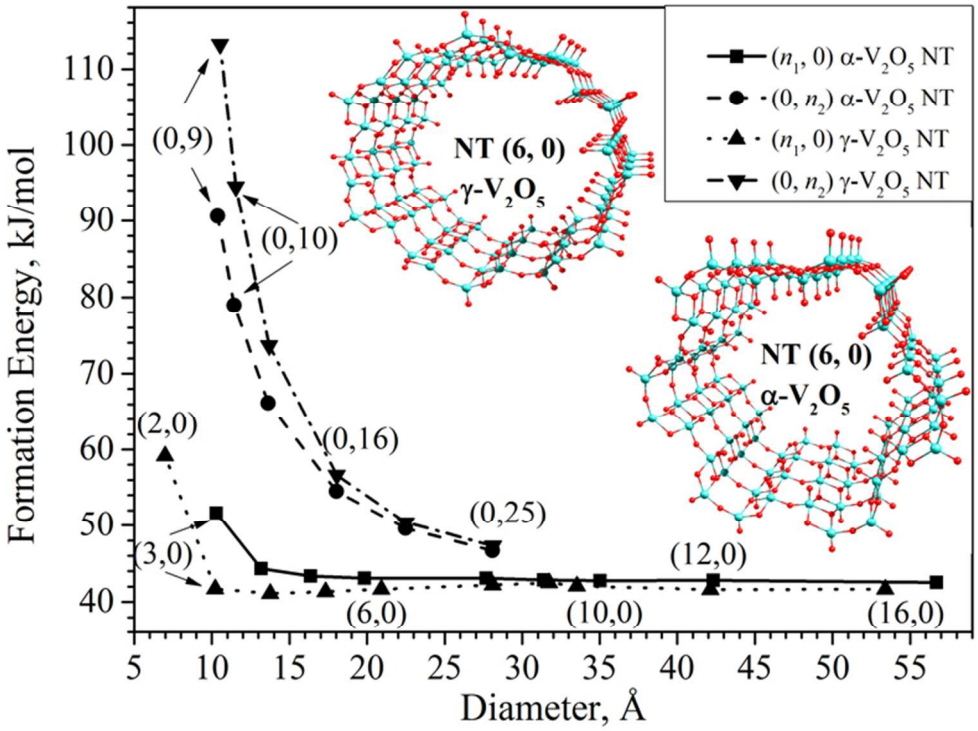

68x50mm (300 x 300 DPI)